Dalton Transactions

PAPER

View Article Online
View Journal | View Issue



Cite this: *Dalton Trans.*, 2014, **43**, 15566

# Synthesis and analysis of the anticancer activity of platinum(II) complexes incorporating dipyridoquinoxaline variants†

Benjamin J. Pages,[a,b] Feng Li,[a,b] Paul Wormell,[b] Dale L. Ang,[a,b] Jack K. Clegg,[c] Cameron J. Kepert,[d] Lawson K. Spare,[a,b] Supawich Danchaiwijit[a,b] and Janice R. Aldrich-Wright*[a,b]

Received 14th July 2014,
Accepted 1st September 2014

DOI: 10.1039/c4dt02133a

www.rsc.org/dalton

Eight platinum(II) complexes with anticancer potential have been synthesised and characterised. These complexes are of the type $[Pt(I_L)(A_L)]^{2+}$, where $I_L$ is either dipyrido[3,2-*f*:2′,3′-*h*]quinoxaline (dpq) or 2,3-dimethyl-dpq (23Me$_2$dpq) and $A_L$ is one of the *R*,*R* or *S*,*S* isomers of either 1,2-diaminocyclohexane (*SS*-dach or *RR*-dach) or 1,2-diaminocyclopentane (*SS*-dacp or *RR*-dacp). The CT-DNA binding of these complexes and a series of other complexes were assessed using fluorescent intercalator displacement assays, resulting in unexpected trends in DNA binding affinity. The cytotoxicity of the eight synthesised compounds was determined in the L1210 cell line; the most cytotoxic of these were [Pt(dpq)(*SS*-dach)]$Cl_2$ and [Pt(dpq)(*RR*-dach)]$Cl_2$, with $IC_{50}$ values of 0.19 and 0.80 μM, respectively. The X-ray crystal structure of the complex [Pt(dpq)(*SS*-dach)]$(ClO_4)_2 \cdot 1.75H_2O$ is also reported.

## Introduction

Chemotherapy is currently the most-utilised treatment for cancer, one of the most globally prominent diseases.[1] Among currently used chemotherapeutics, platinum complexes are held in high regard, with approximately 60% of treatment schemes utilising cisplatin and its analogues.[2] These complexes are known to induce apoptosis in cancerous cells through the formation of DNA adducts, resulting in the cross-linking, bending, and unwinding of the helix.[3] However, these drugs are far from ideal chemotherapeutic agents as their treatment often results in toxic side-effects, and these compounds encounter intrinsic and acquired resistance from many lines of cancerous cells.[4,5] Recent attempts to overcome these limitations have involved the development of non-classical platinum-based chemotherapeutics. These compounds have great potential as chemotherapeutic agents as they are able to both bypass traditional cell resistance mechanisms and exert higher cytotoxicity than cisplatin and its analogues.[6–9]

To this end, our group has developed a large family of platinum(II) complexes (PCs), many of which are more biologically active than cisplatin in many cell lines.[10] The general structure of these complexes is $[Pt(I_L)(A_L)]^{2+}$, where $I_L$ is an aromatic intercalating ligand and $A_L$ is a bidentate ancillary ligand. The nature of these complexes allows for the modulation of their chemical properties *via* the use of different $I_L$ and $A_L$ combinations.[11] These PCs differ from cisplatin in that they will reversibly intercalate between the base pairs of DNA rather than covalently bind.[12] Our most active compound to date, [(5,6-dimethyl-1,10-phenanthroline)(1*S*,2*S*-diaminocyclohexane) platinum(II)] dichloride is up to 100 times more active than cisplatin in a variety of cell lines, with an $IC_{50}$ of 0.009 ± 0.002 μM in the L1210 murine leukaemia cell line.[13] Despite the high activity of these complexes, there is much that is unknown regarding their mechanism of action.[13] A prominent example is that no clear correlation has been found between the DNA binding affinity and the cytotoxicity of these complexes.[11,14,15]

In this study, we have attempted to find such a correlation through both the synthesis of several platinum(II) anticancer complexes and the study of their DNA binding *via* fluorescent intercalator displacement assays (FIDs). The complexes synthesised here incorporated either dipyrido[3,2-*f*:2′,3′-*h*]quinoxaline (dpq) or 2,3-dimethyl-dpq (23Me$_2$dpq) as an $I_L$ and one

[a]*Nanoscale Organisation and Dynamics Group, University of Western Sydney, Locked Bag 1797, Penrith South DC, NSW 2751, Australia.*
*E-mail: j.aldrich-wright@uws.edu.au; Fax: +61 2 4620 3025; Tel: +61 2 4620 3218*
[b]*School of Science and Health, University of Western Sydney, Penrith, NSW 2751, Australia*
[c]*School of Chemistry and Molecular Biosciences, The University of Queensland, St Lucia, QLD 4072, Australia*
[d]*School of Chemistry, The University of Sydney, NSW 2006, Australia*

†Electronic supplementary information (ESI) available: Further synthesis and characterisation data including detailed spectra. CCDC 1008700 for [Pt(dpq)(*SS*-dach)]$(ClO_4)_2 \cdot 1.75H_2O$. For ESI and crystallographic data in CIF or other electronic format see DOI: 10.1039/c4dt02133a

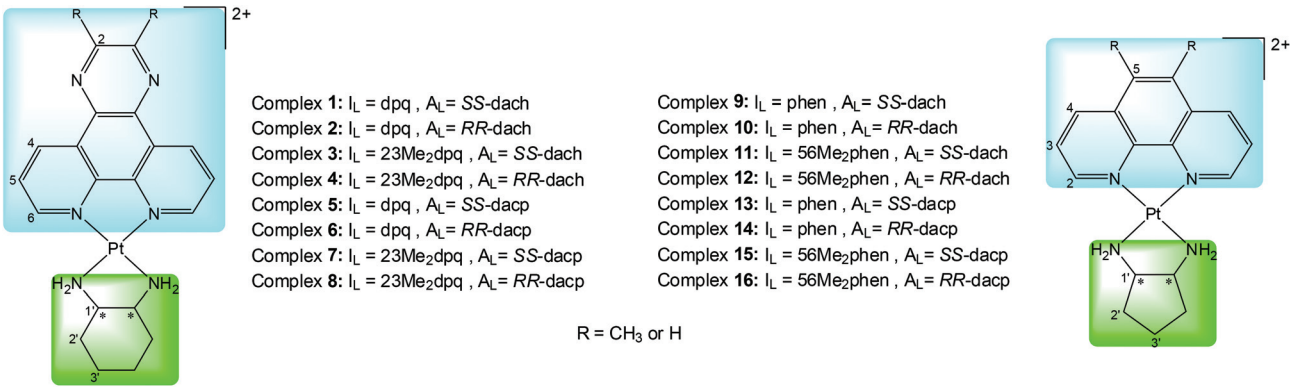


**Fig. 1** The general structure of the PCs investigated here, showing each compound number and their $I_L$ (blue) and $A_L$ (green, * indicates stereo-centres). Also shown is the symmetrical proton numbering system adopted for NMR chemical shift assignment, and counter ions have been omitted for clarity.

of the *R*,*R* or *S*,*S* isomers of either 1,2-diaminocyclohexane (*SS*-dach or *RR*-dach) or 1,2-diaminocyclopentane (*SS*-dacp or *RR*-dacp) as an $A_L$ (Fig. 1). These compounds were synthesised in order to determine the influence of the size of the $I_L$ on the DNA binding affinity and cytotoxicity of these PCs. It was postulated that the use of the larger $I_L$ dpq would result in complexes with higher DNA binding affinity, and subsequently higher cytotoxicity, than the established complexes incorporating 1,10-phenanthroline derivatives. This is due to the larger aromatic surface area of dpq, which could result in stronger π-stacking interactions between the ligand and DNA base-pairs during intercalation.[16] Both dach and dacp were used as $A_L$s as each of these ligands are known to have a different yet positive influence on the cytotoxicity of PCs.[10]

Here we present the synthesis of eight PCs, including [Pt(dpq)(*SS*-dach)]$Cl_2$ (**1**), [Pt(dpq)(*RR*-dach)]$Cl_2$ (**2**), [Pt(23Me$_2$dpq)(*SS*-dach)]$Cl_2$ (**3**), [Pt(23Me$_2$dpq)(*RR*-dach)]$Cl_2$ (**4**), [Pt(dpq)(*SS*-dacp)]$Cl_2$ (**5**), [Pt(dpq)(*RR*-dacp)]$Cl_2$ (**6**), [Pt(23Me$_2$dpq)(*SS*-dacp)]$Cl_2$ (**7**), and [Pt(23Me$_2$dpq)(*RR*-dacp)]$Cl_2$ (**8**). The L1210 murine leukaemia cell line cytotoxicity and calf-thymus DNA (CT-DNA) binding affinity of these complexes were determined and compared to similar complexes incorporating the $I_L$s 1,10-phenanthroline (phen) and 5,6-dimethyl-1,10-phenanthroline (56Me$_2$phen) (Fig. 1). These complexes are [Pt(phen)(*SS*-dach)]$Cl_2$ (**9**), [Pt(phen)(*RR*-dach)]$Cl_2$ (**10**), [Pt(56Me$_2$phen)(*SS*-dach)]$Cl_2$ (**11**), [Pt(56Me$_2$phen)(*RR*-dach)]$Cl_2$ (**12**), [Pt(phen)(*SS*-dacp)]$Cl_2$ (**13**), [Pt(phen)(*RR*-dacp)]$Cl_2$ (**14**), [Pt(56Me$_2$phen)(*SS*-dacp)]$Cl_2$ (**15**) and [Pt(56Me$_2$phen)(*RR*-dacp)]$Cl_2$ (**16**).

# Experimental

## Materials

Reagents were used as received and all solvents were of analytical grade or higher. Dpq and 23Me$_2$dpq were synthesised using published methods.[17,18] *SS*-dach, *RR*-dach, 1*S*,2*S*-diaminocyclopentane-dihydrochloric acid, 1*R*,2*R*-diaminocyclopentane-dihydrochloric acid, dipotassium hydrogen orthophosphate, potassium dihydrogen orthophosphate, potassium perchlorate, sodium chloride, ethylenediamine tetra-acetic acid (EDTA), calf-thymus DNA (CT-DNA) and ethidium bromide were obtained from Sigma-Aldrich chemicals. Acetonitrile and sodium hydroxide were obtained from Merck and methanol was obtained from Lab Scan. Potassium tetrachloroplatinate was obtained from Precious Metals Online. Lastly, deuterated solvents $D_2O$ and DMSO-$d_6$ were obtained from Cambridge Isotope Laboratories.

## Physical measurements

NMR spectra were obtained on a 400 MHz Bruker Avance nuclear magnetic resonance spectrometer, either in $D_2O$ (25 °C) or DMSO-$d_6$ (35 °C), referenced internally to the solvent. $^1$H spectra were obtained using a spectral width of 15 ppm and 256 accumulations. $^1$H-$^{195}$Pt HMQC spectra were obtained using a spectral width of 2500 ppm and 256 data points for the $^{195}$Pt nucleus (F1 dimension), and a spectral width of 12 ppm and 2048 data points for the $^1$H nucleus (F2 dimension). The following abbreviations apply to spin multiplicity: s (singlet), bs (broad singlet), d (doublet), dd (doublet of doublets) t (triplet), and m (multiplet). The chemical shift (parts per million) of each resonance were quoted as an approximate midpoint of its multiplicity.

Mass spectra were obtained on a Waters Micromass ZQ quadrupole mass spectrometer, using the positive electrospray ionisation mode. Samples were prepared in a solution of water and MeCN (1 : 1). Each sample was injected with a cone voltage of 40 V, source temperature of 130 °C and desolvation temperature of 350 °C. Spectra were collected over 1.5 minutes with an *m*/*z* range of 100–1000.

Microelemental analysis (C, H and N) was performed at the Chemical Analysis Facility, Department of Chemistry and Biomolecular Sciences, Macquarie University. An Elemental Analyser, Model PE2400 CHNS/O produced by PerkinElmer, USA, was used.

Electronic spectra were recorded on a Cary 1E spectrophotometer at room temperature in the 200–400 nm range, using

a 10 mm quartz cell. All samples were automatically corrected for solvent baseline.

Circular dichroism spectra were obtained using a Jasco-810 spectropolarimeter at room temperature. The instrument was left to equilibrate for 30 minutes prior to use. Spectra were obtained in a 10 mm quartz cell, and were measured from 400–195 nm with a data pitch of 1 nm, bandwidth of 1 nm and response time of 1 second. For each spectrum, 40 accumulations were collected and a water baseline was subtracted.

High performance liquid chromatography experiments were performed on an Agilent Technologies 1260 Infinity machine, using a Varian Polaris C18-A reverse phase column (4.6 × 250 mm, 5 μm pore size). The mobile phase consisted of formic acid (12.5 mM) in a methanol–water mixture (37 : 64). Elution occurred isocratically with an injection volume of 2.5 μL and a flow rate of 0.8 μL $min^{-1}$. Detection was achieved through a photodiode array, with an absorbance wavelength range of 190–600 nm. An integration threshold height rejection of 5 mAU was used to determine the percentage contribution of each absorbance peak.

### X-ray crystallography

Data collection was performed on an Agilent Technologies SuperNova (Dual Source) System (Mo Kα, $\lambda$ = 071073 Å) equipped with an Oxford Cryosystems nitrogen gas cryostream at 150(2) K. Data was processed using CrysAlisPro.[19] The structures were solved by direct methods using SIR97,[20] then refined and extended with SHELXL-2013 within the WinGX-32 graphical user interface.[21,22] Anisotropic thermal parameters were applied to all non-hydrogen atoms. Carbon-bound hydrogen atoms were included in idealised positions and refined using a riding model. Nitrogen bound hydrogen atoms were first located in the difference Fourier map before refinement, while water hydrogen atoms could not be located and were not included in the model. Three of the perchlorate anions are disordered, each modelled over two equal occupancy positions. A number of bond length and angle restraints were required to facilitate realistic modelling of the disorder. Crystallographic data is summarised in Table 1.†

**Table 1** The crystallographic parameters for [Pt(dpq)(*SS*-dach)]-$(ClO_4)_2$·1.75$H_2O$

| Parameters | Values |
|---|---|
| Empirical formula | $C_{20}H_{22.5}Cl_2N_6O_{9.75}Pt$ |
| Formula weight | 771.95 |
| Temperature/K | 150(2) |
| Crystal system | Monoclinic |
| Space group | $P2_1$(#4) |
| $a$/Å | 8.4187(2) |
| $b$/Å | 16.5210(4) |
| $c$/Å | 18.4677(4) |
| $\alpha$/° | 90.0 |
| $\beta$/° | 100.027(2) |
| $\gamma$/° | 90.0 |
| Volume/Å$^3$ | 2529.36(10) |
| $Z$ | 4 |
| $\rho_{calc}$/mg $mm^{-3}$ | 2.027 |
| $\mu$/$mm^{-1}$ | 5.824 |
| $F$(000) | 1510 |
| Crystal size/mm | 0.2 × 0.1 × 0.1 |
| Theta range for data collection | 2.872 to 29.641° |
| Index ranges | $-10 \le h \le 10$, $-21 \le k \le 20$, $-24 \le l \le 24$ |
| Reflections collected | 29 166 |
| Independent reflections | 11 520 [$R$(int) = 0.0488] |
| Data/restraints/parameters | 11 520/135/2692 |
| Goodness-of-fit on $F^2$ | 1.029 |
| Final $R$ indexes [$I > 2\sigma(I)$] | $R_1$ = 0.0504, w$R_2$ = 0.1095 |
| Final $R$ indexes [all data] | $R_1$ = 0.0902, w$R_2$ = 0.1316 |
| Flack parameter | 0.014(10) |
| Largest diff. peak/hole/e Å$^{-3}$ | 3.028/−1.944 |

### Fluorescent intercalator displacement assays

The binding of complexes **1–16** to CT-DNA was analysed through monitoring of the fluorescence of a solution of ethidium-bound CT-DNA in buffer (5 mM $K_2HPO_4$–$KH_2PO_4$, 50 mM NaCl, 1 mM EDTA). The stock CT-DNA (220 μM) and ethidium bromide (441 μM) solution concentrations were confirmed using the extinction coefficients of $\varepsilon_{260}$ = 13200 $M^{-1}$ $cm^{-1}$ per base pair and $\varepsilon_{476}$ = 5680 $M^{-1}$ $cm^{-1}$, respectively.[23,24] These stock solutions were combined with solutions of PC and buffer as per Table S4.1,† and the emission intensities at 601 nm were recorded. Emission was measured using a Varian Cary Eclipse fluorescence spectrophotometer. Samples were measured in a 96 well plate with a sample volume of 250 μL. The excitation wavelength was 530 nm, and fluorescence intensity was measured from 550–750 nm with a 1 nm data interval, a scan rate of 600 nm $min^{-1}$ and an averaging time of 0.1 s. The excitation and emission slits were set to 5 nm and 10 nm, respectively, and all experiments were performed at room temperature in duplicate.

### *In vitro* growth inhibition assays

*In vitro* growth inhibition assays of the synthesised complexes and cisplatin were performed at the Peter MacCallum institute in Melbourne, Victoria, Australia. Each complex was dissolved in water before being diluted with the appropriate cell media to the required concentration. The experiments were performed in the L1210 murine leukaemia cell line using the Coulter Counting Assay. For each complex, two independent experiments were performed, each with an exposure time of 48 h.

### General synthesis of $[Pt(I_L)(A_L)]Cl_2$

Synthesis was achieved using an adaptation of the published method.[25] $K_2PtCl_4$ (218 mg, 0.53 mmol) and $A_L$ (1 equiv.) were combined and stirred in water (10 mL), and cooled at 4 °C for 24 h. The ligand dacp was obtained as a dihydrochloride salt, and so in this case it was dissolved in water separately and the pH of the solution increased to ~10 using sodium hydroxide before the addition of $K_2PtCl_4$. The resultant precipitate was collected by vacuum filtration and washed (with water, ethanol and diethyl ether, each 10 mL) to obtain the yellow product $[Pt(A_L)Cl_2]$ (Yield 89%). This product was refluxed (110 °C, 2 d) with the $I_L$ (1.1 equiv.). The volume of the solution was reduced under pressure by ~50% before reflux for another 2 d. The solution was cooled overnight to precipitate excess $I_L$ and

 

Table 2 Summary of the characterisation data of complexes **1–8**

| No. | Molecular formula | Yield (%) | ESI-MS ($m/z$) $[M - H]^+$ Calc. (Found) | Microanalysis Calc. (Found) C | H | N | UV/$\lambda_{max}$ (nm) ($\varepsilon$/mol$^{-1}$ dm$^3$ cm$^{-1}$) × $10^3$ | CD/$\lambda_{max}$ (nm) (mdeg L mol$^{-1}$) × $10^{-1}$ | HPLC peak area |
|---|---|---|---|---|---|---|---|---|---|
| 1 | [Pt(dpq)(*SS*-dach)]$Cl_2$·$2H_2O$ | 86 | 540.2 (539.6) | 37.04 (37.21) | 4.04 (3.76) | 12.96 (12.96) | 257 (50), 348 (4) | 204 (−24), 227 (15), 257 (−18), 300 (−11), 339 (5) | >99% |
| 2 | [Pt(dpq)(*RR*-dach)]$Cl_2$·$2H_2O$ | 74 | 540.2 (539.4) | 37.04 (37.23) | 4.04 (3.72) | 12.96 (12.97) | 258 (50), 348 (4) | 204 (20), 226 (−15), 256 (23), 300 (15), 339 (−5) | >99% |
| 3 | [Pt(23$Me_2$dpq)(*SS*-dach)]$Cl_2$·$4H_2O$ | 61 | 568.2 (567.0) | 37.08 (36.77) | 4.81 (4.69) | 11.79 (11.72) | 226 (23), 261 (45), 356 (4) | 202 (−22), 228 (13), 260 (−14), 271 (−1), 288 (−11), 335 (6) | >98% |
| 4 | [Pt(23$Me_2$dpq)(*RR*-dach)]$Cl_2$·$4H_2O$ | 57 | 568.2 (567.5) | 37.08 (37.27) | 4.81 (4.76) | 11.79 (11.81) | 226 (24), 261 (46), 356 (4) | 204 (22), 228 (−11), 259 (23), 267 (8), 285 (18), 335 (−6) | >98% |
| 5 | [Pt(dpq)(*SS*-dacp)]$Cl_2$·$3H_2O$ | 73 | 526.1 (525.0) | 34.98 (34.55) | 4.02 (3.81) | 12.88 (12.80) | 257 (46), 348 (4) | 203 (−27), 228 (12), 259 (−8), 275 (3), 302 (−11), 341 (5) | >99% |
| 6 | [Pt(dpq)(*RR*-dacp)]$Cl_2$·$3H_2O$ | 76 | 526.1 (525.3) | 34.98 (34.82) | 4.02 (3.81) | 12.88 (12.81) | 257 (47), 348 (4) | 204 (29), 230 (−14), 256 (15), 275 (2), 303 (13), 340 (−6) | >99% |
| 7 | [Pt(23$Me_2$dpq)(*SS*-dacp)]$Cl_2$·$3.5H_2O$ | 57 | 554.1 (553.6) | 36.58 (36.60) | 4.53 (4.31) | 12.19 (12.19) | 226 (23), 261 (44), 356 (4) | 200 (−26), 228 (12), 258 (−10), 271 (5), 296 (−8), 339 (7) | >99% |
| 8 | [Pt(23$Me_2$dpq)(*RR*-dacp)]$Cl_2$·$3.5H_2O$ | 58 | 554.1 (553.2) | 37.58 (36.65) | 4.53 (4.32) | 12.19 (12.23) | 226 (24), 261 (46), 356 (4) | 202 (24), 229 (−9), 259 (15), 270 (2), 295 (10), 335 (−7) | >99% |

filtered through a 0.45 μm filter using a syringe. The volume was then reduced to ~3 mL through rotary evaporation. To purify, a Sep-Pak® (20 cc, 2 g) was activated through the elution of methanol (15 mL) and water (30 mL). The $[Pt(I_L)(A_L)]Cl_2$ solution was loaded onto the column and eluted with water. The first 10 mL to elute was discarded and the remaining yellow band was collected, leaving an orange band at the head of the column. This solution was lyophilised to produce a pale yellow solid. NMR data is reported in Table 2 while yield and other characterisation data are presented in Table 3. Crystals of the complex $[Pt(dpq)(SS\text{-dach})](ClO_4)_2$·$1.75H_2O$ were produced by the addition of $KClO_4$ to a concentrated solution of complex **1** in water, followed by the slow evaporation of the solvent.

# Results and discussion

### Synthesis and characterisation

The synthesis of complexes **1–8** was achieved *via* adaptation of published methods.[25] Firstly, the water-soluble $K_2PtCl_4$ and $A_L$ were reacted to form the water-insoluble product $[Pt(A_L)Cl_2]$, which was easily isolated *via* filtration. Secondly, this complex was refluxed with the desired $I_L$ to produce $[Pt(I_L)(A_L)]Cl_2$. This reflux method is commonly used for complexes of this type; however, dpq and 23$Me_2$dpq are less water-soluble than phen and so even with reflux periods spanning up to four days, undissolved $I_L$ and $[Pt(A_L)Cl_2]$ remained once the reaction solution was cooled. This resulted in yields that were typically 10–20% lower than previous syntheses.[10] However, the higher

Table 3 Summary of NMR data of complexes **1–8**, showing chemical shift (ppm), integration, multiplicity and coupling constants for the eight complexes synthesised. Experiments were performed in $D_2O$, and so amine resonances were not observed due to proton exchange

| | Complex no. | | | | | | | |
|---|---|---|---|---|---|---|---|---|
| Label | **1** | **2** | **3** | **4** | **5** | **6** | **7** | **8** |
| H2 | 9.20 (2H, s) | 9.20 (2H, s) | — | — | 9.20 (2H, s) | 9.20 (2H, s) | — | — |
| H4 | 9.75 (2H, d, $J$ = 8.44 Hz) | 9.75 (2H, d, $J$ = 8.40 Hz) | 9.59 (2H, d, $J$ = 8.50 Hz) | 9.27 (2H, d, $J$ = 8.50 Hz) | 9.74 (2H, d, $J$ = 8.38 Hz) | 9.75 (2H, d, $J$ = 8.45 Hz) | 9.35 (2H, d, $J$ = 8.35 Hz) | 9.40 (2H, d, $J$ = 8.37 Hz) |
| H5 | 8.16 (2H, dd, $J$ = 8.26, 5.62 Hz) | 8.17 (2H, dd, $J$ = 8.36, 5.52 Hz) | 8.14 (2H, dd, $J$ = 7.86, 5.93 Hz) | 8.13 (2H, dd, $J$ = 8.06, 5.56 Hz) | 8.15 (2H, dd, $J$ = 8.42, 5.56 Hz) | 8.15 (2H, dd, $J$ = 7.53, 6.02 Hz) | 8.17 (2H, dd, $J$ = 7.94, 5.80 Hz) | 8.16 (2H, dd, $J$ = 7.85, 5.87 Hz) |
| H6 | 9.03 (2H, d, $J$ = 5.46 Hz) | 9.03 (2H, d, $J$ = 5.30 Hz) | 8.97 (2H, d, $J$ = 5.67 Hz) | 8.97 (2H, d, $J$ = 5.67 Hz) | 8.91 (2H, d, $J$ = 5.50 Hz) | 8.92 (2H, d, $J$ = 5.51 Hz) | 8.85 (2H, d, $J$ = 5.12 Hz) | 8.87 (2H, d, $J$ = 5.32 Hz) |
| H1′ | 2.72 (2H, m) | 2.72 (2H, m) | 2.73 (2H, m) | 2.75 (2H, m) | 3.56 (2H, m) | 3.56 (2H, m) | 3.60 (2H, m) | 3.60 (2H, m) |
| $H2'_{eq}$ | 2.22 (2H, d, $J$ = 12.10 Hz) | 2.22 (2H, d, $J$ = 12.48 Hz) | 2.23 (2H, d, $J$ = 11.97 Hz) | 2.24 (2H, d, $J$ = 12.59 Hz) | — | — | — | — |
| $H3'_{eq}$ | 1.65 (2H, m) | 1.65 (2H, m) | 1.66 (2H, m) | 1.65 (2H, m) | — | — | — | — |
| $H2'_{ax}$ | 1.47 (2H, m) | 1.47 (2H, m) | 1.49 (2H, m) | 1.50 (2H, m) | — | — | — | — |
| $H3'_{ax}$ | 1.23 (2H, m) | 1.24 (2H, m) | 1.24 (2H, m) | 1.26 (2H, m) | — | — | — | — |
| H3′ | — | — | — | — | 2.31 (2H, m) | 2.31 (2H, m) | 2.34 (2H, m) | 2.34 (2H, m) |
| $H2'_{ax/eq}$ | — | — | — | — | 1.95 (2H, m) | 1.95 (2H, m) | 1.98 (2H, m) | 1.98 (2H, m) |
| $H2'_{ax/eq}$ | — | — | — | — | 1.58 (2H, m) | 1.58 (2H, m) | 1.63 (2H, m) | 1.62 (2H, m) |
| $-CH_3$ | — | — | 2.83 (6H, s) | 2.83 (6H, s) | — | — | 2.80 (6H, s) | 2.81 (6H, s) |
| $^1H/^{195}Pt$ | 9.12/−2812.6 | 9.13/−2812.6 | 9.07/−2792.6 | 9.08/−2792.6 | 9.01/−2548.2 | 9.02/−2548.2 | 8.97/−2539.8 | 8.97/−2539.8 |

aromaticity of complexes **1–8** did assist Sep-Pak® purification; the final product was retained on the column for longer, allowing an impurity to elute first. NMR experiments determined that this impurity was unreacted $[Pt(A_L)Cl_2]$, and so this fraction was discarded (section S1.1†).

Each complex was characterised by a combination of NMR (sections S2.3 and S2.4†), electrospray ionization mass spectrometry (ESI-MS, section S2.5†), high performance liquid chromatography (HPLC, section S2.6†), microanalysis, circular dichroism (CD) spectroscopy (section S2.2†) and ultraviolet (UV) spectroscopy (section S2.1†). The NMR spectra produced by each complex showed the expected resonances and little to no traces of impurity. The ESI-MS spectra confirmed the presence of the predicted parent ion (Table 2). The purity of each complex was determined to be over 98% as per analysis of the HPLC peak area and this was confirmed by the closeness of the microanalysis data to the calculated values (Table 2). The retention of chirality of the complexes during synthesis was confirmed by CD spectra.

### NMR spectral assignment

NMR characterisation of each PC was achieved using a combination of $^1$H NMR and $^1$H-$^{195}$Pt heteronuclear multiple quantum correlation (HMQC) spectra (Table 3). As an example, the labelled $^1$H NMR spectrum of complex **1** is shown (Fig. 2). Regarding the aromatic region, complex **1** produced a singlet at 9.20 ppm; this was assigned H2 as there is no proton bound to the adjacent carbon. The resonance at 8.16 ppm was assigned H5 as the coupling of these protons to both H4 and H6 would produce the observed doublet of doublets splitting pattern.

To distinguish between the remaining aromatic doublets, their coupling constants were compared; in pyridyl ring systems, the proton located on the carbon in the alpha position relative to nitrogen produces a smaller coupling constant than protons in the H4 position.[26] Therefore, the doublet at 9.03 ppm with $J$ = 5.46 Hz was assigned H6 and the doublet at 9.75 ppm with $J$ = 8.44 Hz was assigned H4. The resonances in the aliphatic region were in agreement with previously published complexes with the same range of $A_L$s, and so peak

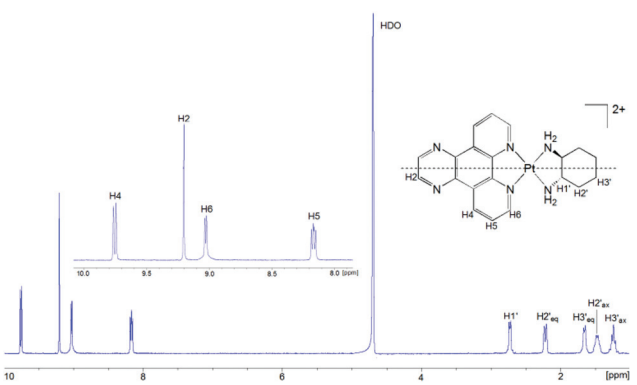


Fig. 2 The $^1$H NMR spectrum of complex **1** in $D_2O$, showing proton assignment.

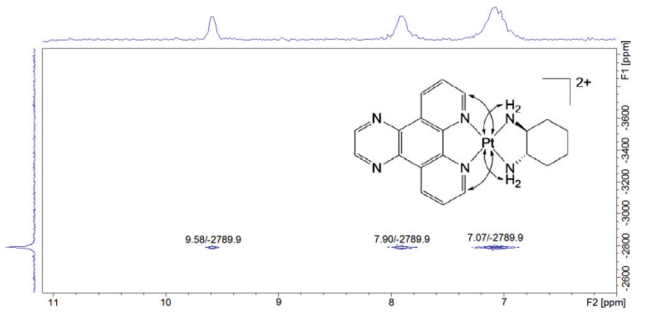


Fig. 3 The $^1$H–$^{195}$Pt HMQC spectrum of complex **1** in DMSO-$d_6$, displaying the correlations between the platinum centre and the protons from each ligand.

assignment was identical to the literature.[10,27] The amine proton resonances were not present in this spectrum due to exchange with $D_2O$. In the proton-platinum HMQC spectrum of complex **1** (Fig. 3), the $^{195}$Pt chemical shift of −2812.6 ppm is very different from those of $[Pt(SS\text{-dach})Cl_2]$ and $K_2PtCl_4$ (−3282 ppm and −1650 ppm, respectively).[10] This is indicative of the presence of a single platinum complex that differs greatly from the starting reagents. Secondly, the correlation between the aromatic resonance at 9.58 ppm and the platinum centre suggests that the $I_L$ has coordinated. Finally, there are correlations between the platinum centre and the proton resonances at 7.90 ppm and 7.07 ppm. These peaks were not present in the $D_2O$ $^1$H NMR spectrum, and so they resulted from the amines of the *SS*-dach $A_L$. These correlations therefore confirm the coordination of each ligand to the platinum centre.

The above methodology was used to assign the NMR spectra of each of complexes **2–8** (S2.3†). However, some minor differences in the NMR spectra of these complexes were observed. In the $^1$H NMR spectrum of complexes incorporating 23Me$_2$dpq, the resonance at 9.20 ppm was replaced by a singlet at ∼2.82 ppm; this peak was assigned as the methyl protons due to the relative integral of six and the singlet multiplicity. The $^{195}$Pt chemical shifts of complexes **5–8** were found to be approximately 250 ppm higher than those of complexes **1–4**. $^{195}$Pt is known to be extremely sensitive to small changes in chemical structure,[28] and so this difference in chemical shift is possibly due to the high ring strain of the dacp $A_L$ relative to dach.[29]

### UV spectra

The UV absorption spectrum of each of the complexes was similar, and the choice of $A_L$ had little effect. Each spectrum was dominated by a strong absorption band at ∼260 nm, with a series of shoulders extending down to a weak band at ∼350 nm (Fig. 4). These bands are attributed to ligand-centred π–π* transitions of the dpq and 23Me$_2$dpq ligands; the weak n–π* transitions are likely to be suppressed in a hydrogen-bonding solvent. These bands are consistent with our own semiempirical CNDO/S-CI calculations for dpq, using the program of Del Bene *et al.*,[30] with the updated code of

 

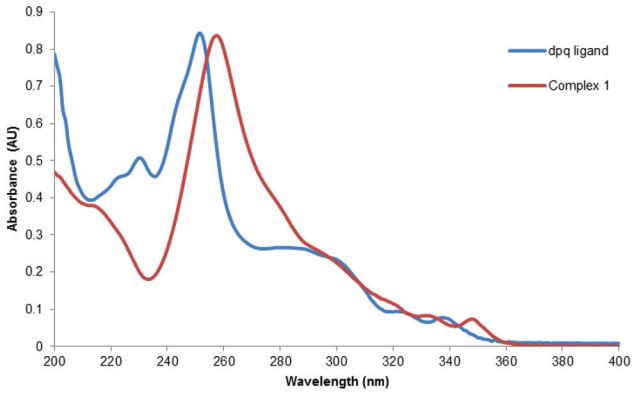


Fig. 4 UV absorption spectra of complex **1** (water) and free dpq (ethanol).

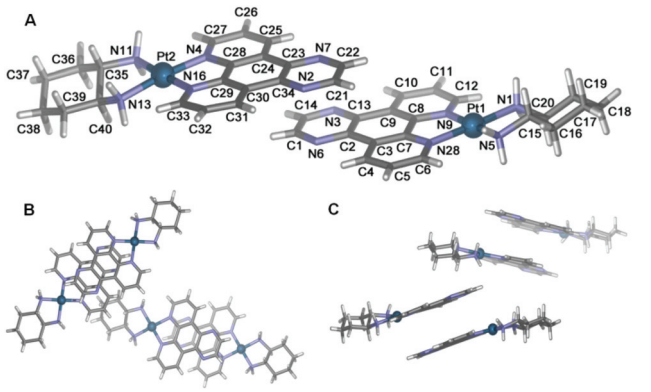


Fig. 5 The X-ray structure of [Pt(dpq)(*SS*-dach)]$(ClO_4)_2$·1.75$H_2O$, showing the atom numbering system (A) and top (B) and side (C) packing views. The metal centres are shown in cerulean, the nitrogen atoms in blue, the carbon in grey and hydrogen atoms in white; perchlorate anions and water molecules have been omitted for clarity.

Reimers, with input geometries from B3LYP/6-31+G** calculations using Gaussian 03.[31] The CNDO/S-CI program is parameterized for compounds of this general class, and performs satisfactorily with low computational cost.

As shown in Fig. 4, the free ligand has a strong absorption centred about 250 nm, weaker absorption around 290 nm, and weak bands beginning at about 340 nm. A comparison between the spectra of the complexes and the free ligand shows a marked red-shift and loss of structure upon complexation. This behaviour parallels that for 1,10-phenanthroline when complexed by platinum(II),[32] and the redshift resembles that for protonated ligands such as 2,2′-dipyridine[33] and 1,10-phenanthroline.[34] We have attempted to reproduce this behaviour for dpq, but have been unable to produce sufficient concentrations of the protonated ligand in water. The complexes incorporating 23$Me_2$dpq exhibited a distinct peak at 226 nm, rather than a shoulder; this feature has not been observed in the UV spectra of complexes incorporating phen and 56$Me_2$phen.[10]

### X-Ray crystal structure of [Pt(dpq)(*SS*-dach)]$(ClO_4)_2$·1.75$H_2O$

The perchlorate salt of the complex $[Pt(dpq)(SS\text{-dach})]^{2+}$ crystallises in the monoclinic chiral space group $P2_1$ with two molecules in the asymmetric unit. It features a square planar metal centre and an $N_4$-coordination sphere (Fig. 5). The relevant bond lengths and angles, as well as the N–C–C–N torsion angles in the complex, are shown in Table 4. The average N–Pt–N bond angles of both dpq and *SS*-dach ligands while coordinated to the platinum centre were 81.2° and 83.0°, respectively. The average Pt–N bond lengths from the dpq and *SS*-dach ligands to the platinum centre were determined to be 2.025 and 2.043 Å, respectively. These results are consistent with those found in crystal structures of similar complexes.[35,36] The N–C–C–N torsion angles (Table 4) for the complex, which were observed as 2(2)° and 5(2)°, revealed a slight distortion upon coordination in the planarity of the dpq ligands.

Upon coordination to the platinum centre, the *SS*-dach ancillary ligand assumed the stable chair conformation, resulting in a puckered six-membered chelate ring in the δ-conformation.[37] This was evident by the positive values of the average N–C–C–N torsion angles (Table 4) which was 54.3°. These angles confirm the stereochemistry of the $A_L$ as *S*,*S*. Additionally, the Flack parameter of 0.014(10) confirms the absolute structure of the complex and the stereochemistry of the ligands.[38] Adjacent dpq ligands stack parallel to the crystallographic *b*-axis with carbon-carbon distances in the range of 3.4–3.5 Å, indicating the presence of π-interactions (Fig. 5).[39] The amine groups form a number of hydrogen bonds with both the perchlorate anions and the solvent water molecules. Intuitively, the number of associated water molecules determined by the elemental microanalysis correlates with the number determined by this crystal structure.

Table 4 Selected bond distances and angles for the complex [Pt(dpq)(*SS*-dach)]$(ClO_4)_2$·1.75$H_2O$, as determined by X-ray crystallography. Standard deviations are shown in parentheses

| Bond distances (Å) | | | |
|---|---|---|---|
| Pt1–N1 | 2.027(15) | Pt2–N4 | 2.003(15) |
| Pt1–N5 | 2.066(13) | Pt2–N11 | 2.035(11) |
| Pt1–N9 | 2.021(13) | Pt2–N13 | 2.042(16) |
| Pt1–N28 | 2.049(16) | Pt2–N16 | 2.025(11) |
| **Bond angles and torsion angles (°)** | | | |
| N9–Pt1–N1 | 97.8(5) | N16–Pt2–N11 | 178.0(5) |
| N9–Pt1–N28 | 80.9(6) | N16–Pt2–N13 | 176.8(5) |
| N1–Pt1–N28 | 177.9(6) | N1–Pt2–N5 | 96.7(5) |
| N9–Pt1–N5 | 173.3(5) | N11–Pt2–N13 | 82.7(5) |
| N1–Pt1–N5 | 83.2(6) | N1–C20–C15–N5 | 56.0(18) |
| N28–Pt1–N5 | 98.3(6) | N4–C28–C29–N16 | 2(2) |
| N4–Pt2–N16 | 81.5(5) | N28–C7–C8–N9 | 5(2) |
| N4–Pt2–N11 | 99.0(5) | N11–C35–C40–N13 | 52.5(16) |

### Fluorescent intercalator displacement (FID) assays

Changes in the emission of fluorescent species during binding events is an efficient way to determine the apparent binding constant, $K_{app}$, for the interactions of compounds with

biomolecules such as proteins and DNA.[40–42] As such, fluorescence spectroscopy was utilised in this study to investigate the interactions of complexes **1–16** with CT-DNA. Fluorescent intercalator displacement assays (FIDs) were used as neither the PCs or CT-DNA are intrinsically fluorescent. In these assays, CT-DNA solutions are bound with ethidium bromide (EtBr), a compound known to exhibit fluorescence only when bound with DNA.[43] The addition of a competitively binding PC results in the displacement of bound EtBr and a subsequent loss in emission of the solution. Therefore, changes in emission upon the incremental addition of these competitive binders can be used to calculate $K_{app}$. EtBr is postulated to occupy more than one binding site of DNA with an overall $K_{app}$ of $\sim 10^5$ M.[44,45] Therefore, the PC $K_{app}$ values calculated from FIDs are an average of the PC-DNA affinity across each of the sites from which EtBr is displaced.

For the FID assays in this study, a series of solutions were measured in which the CT-DNA and EtBr concentrations were kept constant while the amount of complexes **1–16** was incrementally increased (Table S3.1†). The addition of each PC to EtBr-bound CT-DNA resulted in a quenching of the fluorescence signal, indicating that each of the complexes displaced EtBr from the base-pair binding sites. Intuitively, the attenuation of emission was larger for higher PC concentrations. This can clearly been seen in Fig. 6 in which the addition of complex **1** to EtBr-bound DNA has resulted in the attenuation of the peak at 601 nm. All of the complexes in the study produced similar emission spectra (section S3.2†).

Prior to the calculation of binding constants from this data, the nature of the fluorophore and quencher interactions had to be determined. Quenching of fluorescence can occur *via* several processes, including energy transfer, excited-state reactions, collisional quenching and static quenching.[46]

Collisional quenching occurs when the fluorophore and quencher interact during the excitation of the fluorophore, whereas static quenching occurs during the formation of a fluorophore-quencher complex in the ground state.[46] The Stern–Volmer equation describes the relationship between the fluorescence of a fluorophore (ethidium-bound CT-DNA) and concentration of quencher (the PC) in solution:[47]

$$\frac{F_0}{F} = 1 + K_q \tau_0 [\mathrm{PC}] = 1 + K_{SV}[\mathrm{PC}] \quad (1)$$

where $F_0$ is the fluorescence of the binding site in the absence of quencher, $F$ is the fluorescence of the site containing the PC, $K_q$ is the bimolecular quenching constant, $\tau_0$ is the lifetime of the chromophore in the absence of the quencher ($23 \times 10^{-9}$ s for ethidium-bound DNA),[48] and $K_{SV}$ is the Stern–Volmer quenching constant. $K_{SV}$ can be determined from the slope of a plot of $F^{-1}/F_0$ against [PC], and $K_q$ can subsequently be determined from $K_{SV}$ and $\tau_0$. If the calculated $K_q$ is $\sim 2 \times 10^{10}$ $M^{-1}$ $s^{-1}$, the fluorescence has been quenched through collisional means, whereas a $K_q$ above the same value indicates that static quenching has occurred.[49] Using Stern–Volmer plots, $K_q$ was calculated for each complex (Table S3.3†). Each value was above $2 \times 10^{10}$ $M^{-1}$ $s^{-1}$, indicating that the quenching of EtBr by each PC occurs statically rather than dynamically; that is, quenching occurs when the PC-DNA complex forms through displacement of EtBr. Due to the static nature of quenching, the displacement of ethidium by each PC can be represented by:

$$n\mathrm{PC} + B_E \rightarrow nB_M + \mathrm{EtBr} \quad (2)$$

where $n$ is the number of DNA binding sites from which a PC has displaced EtBr, and $B_E$ and $nB_M$ represent DNA that is bound by EtBr and $n$ molecules of PC, respectively. During the calculation of $K_{app}$, it is typically assumed that each EtBr molecule is permanently displaced from the DNA binding site, therefore having no effect on the $K_{app}$ of the quencher.[50–52] The $K_{app}$ for this interaction can therefore be written as:

$$K_{app} = \frac{[nB_M]}{[\mathrm{PC}]^n [B_E]} \quad (3)$$

During the displacement process, the initial concentration of EtBr-bound binding sites, $B_{E_0}$, is equal to the total concentration of the PC-bound and EtBr-bound sites through eqn (4):

$$[B_{E_0}] = [B_E] + [nB_M] \quad (4)$$

The ratio between concentration and fluorescence ($F$) of $B_E$ and $B_{E_0}$ is represented by:

$$\frac{[B_E]}{[B_{E_0}]} = \frac{[F]}{[F_0]} \quad (5)$$

Manipulation of these expressions reveals the logarithmic relationship, eqn (6):

$$\log_{10}\left(\frac{F_0 - F}{F}\right) = n \log_{10}[\mathrm{PC}] + \log_{10} K_{app} \quad (6)$$

Therefore, the double-logarithm plot of $\log_{10}(F_0 - F/F)$ against $\log_{10}[\mathrm{PC}]$ can be used to determine $K_{app}$ and $n$ from the intercept and slope, respectively. The plots generated for each complex (section S3.2†) were linear over the entire

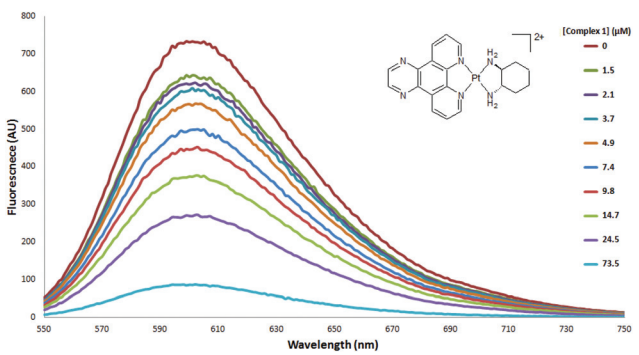


**Fig. 6** Emission spectra of CT-DNA (73.5 μM) and EtBr (29.4 μM) with increasing concentration of complex **1**. [$K_2HPO_4$–$KH_2PO_4$] = 5 mM, [NaCl] = 50 mM, [EDTA] = 1 mM.

 

Table 5 Summary of the binding data obtained from the double-logarithm plots of the PCs tested. Standard errors (±) are quoted to two decimal places

| No. | $n$ | $K_{app}/M^{-1}$ | No. | $n$ | $K_{app}/M^{-1}$ |
|---|---|---|---|---|---|
| 1 | 1.12 ± 0.03 | $(1.9 \pm 0.1) \times 10^5$ | 9 | 0.79 ± 0.01 | $(1.88 \pm 0.01) \times 10^3$ |
| 2 | 1.16 ± 0.01 | $(3.5 \pm 0.7) \times 10^5$ | 10 | 0.8 ± 0.1 | $(4.0 \pm 0.1) \times 10^3$ |
| 3 | 1.14 ± 0.02 | $(2.9 \pm 0.5) \times 10^5$ | 11 | 1.35 ± 0.01 | $(2.1 \pm 0.3) \times 10^6$ |
| 4 | 1.17 ± 0.09 | $(3.9 \pm 0.4) \times 10^5$ | 12 | 1.35 ± 0.01 | $(2.4 \pm 0.5) \times 10^6$ |
| 5 | 1.07 ± 0.01 | $(1.18 \pm 0.01) \times 10^5$ | 13 | 0.87 ± 0.02 | $(4.8 \pm 0.2) \times 10^3$ |
| 6 | 1.10 ± 0.01 | $(1.40 \pm 0.09) \times 10^5$ | 14 | 0.8 ± 0.1 | $(3.0 \pm 0.7) \times 10^3$ |
| 7 | 1.17 ± 0.01 | $(3.7 \pm 0.1) \times 10^5$ | 15 | 1.30 ± 0.01 | $(1.15 \pm 0.09) \times 10^6$ |
| 8 | 1.19 ± 0.02 | $(3.47 \pm 0.07) \times 10^5$ | 16 | 1.45 ± 0.04 | $(1.7 \pm 0.1) \times 10^6$ |

concentration range tested; a summary of the data determined for each PC is shown in Table 5.

It can be seen that each of the MCs tested displayed a high affinity for CT-DNA, with a range of $K_{app}$ values from $10^3$–$10^7$ $M^{-1}$. For complexes **9–16**, the use of 56Me$_2$phen as an $I_L$ resulted in a much higher DNA binding affinity than the use of phen. Interestingly, $K_{app}$ values for complexes **1–8** were all similar, suggesting that the methyl substituents did not impact DNA binding affinity (Fig. 7).

A generally positive correlation between $K_{app}$ and $n$ was observed, which intuitively indicates that the complexes with higher DNA binding affinity were able to displace a higher number of EtBr molecules. The complexes incorporating dpq (**1**, **2**, **5**, **6**) demonstrated much higher binding affinities than those incorporating phen (**9**, **10**, **13**, **14**). This is thought to be due to the larger aromatic surface of the dpq $I_L$, as it contains a higher density of π-electrons that can stack with the base-pairs in the binding site. However, the same trend was not observed in complexes that incorporated the methylated intercalating ligands; the 56Me$_2$phen complexes (**11**, **12**, **15**, **16**) bound to CT-DNA with greater affinity than those incorporating both dpq and 23Me$_2$dpq (**1–8**). This suggests that the structure of the 56Me$_2$phen $I_L$ is the optimum size when it comes to DNA binding affinity.

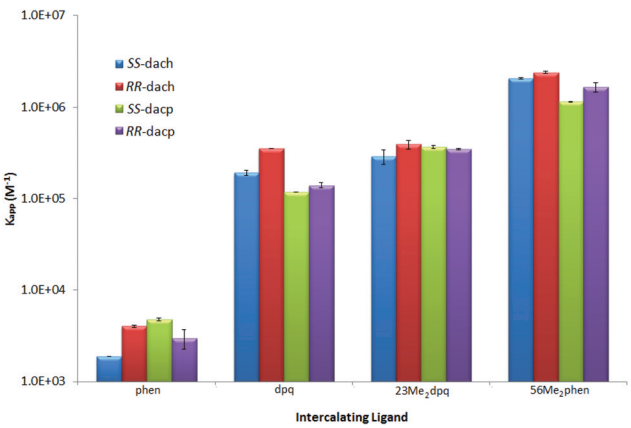


Fig. 7 Comparison of the CT-DNA binding affinity of complexes **1–16**, represented by the calculated $K_{app}$ with standard error.

Contrary to what has been determined here, a previous study of the DNA binding affinity of a range of complexes with varied surface areas has determined that some dpq complexes do not bind to CT-DNA with a higher affinity than phen complexes.[11] However, this study utilised circular dichroism (CD) spectroscopy to analyse PC-DNA binding rather than FIDs. It is clear that different spectroscopic techniques and assay conditions may produce different results;[53–55] further investigation into these differences and DNA binding trends is warranted.

### *In vitro* cytotoxicity

The biological activity of complexes **1–8** were determined in the L1210 murine leukaemia cell line in order to compare them to previously studied complexes of this type. Despite the similarities in chemical structure, complexes **1–8** produced a wide variety of $IC_{50}$ values (Table 6, Fig. 8). As per the pre-

Table 6 *In vitro* cytotoxicity of complexes **1–16** in the L1210 murine leukaemia cell line, expressed as $IC_{50}$ values with standard error. PC activity was also compared to cisplatin

| Complex no. | $I_L$ | $A_L$ | $IC_{50}/\mu M$ | $IC_{50}$ (*SS–RR*) | Comparison complex no. | $I_L$ | $A_L$ | $IC_{50}/\mu M$[a] | $IC_{50}$ (*SS–RR*) |
|---|---|---|---|---|---|---|---|---|---|
| 1 | dpq | *SS*-dach | 0.19 ± 0.01 | −0.61 | 9 | Phen | *SS*-dach | 0.10 ± 0.01 | −1.40 |
| 2 | dpq | *RR*-dach | 0.80 ± 0.20 | | 10[b] | Phen | *RR*-dach | 1.50 ± 0.10 | |
| 3 | 23Me$_2$dpq | *SS*-dach | 1.30 ± 0.40 | −4.70 | 11 | 56Me$_2$phen | *SS*-dach | 0.009 ± 0.002 | −0.451 |
| 4 | 23Me$_2$dpq | *RR*-dach | 6.00 ± 2.00 | | 12 | 56Me$_2$phen | *RR*-dach | 0.46 ± 0.01 | |
| 5 | dpq | *SS*-dacp | 4.10 ± 0.90 | 1.85 | 13 | Phen | *SS*-dacp | 2.80 ± 0.30 | 1.20 |
| 6 | dpq | *RR*-dacp | 2.25 ± 0.07 | | 14 | Phen | *RR*-dacp | 1.60 ± 0.01 | |
| 7 | 23Me$_2$dpq | *SS*-dacp | 4.20 ± 0.80 | −0.80 | 15 | 56Me$_2$phen | *SS*-dacp | 0.23 ± 0.03 | 0.06 |
| 8 | 23Me$_2$dpq | *RR*-dacp | 5.00 ± 1.00 | | 16 | 56Me$_2$phen | *RR*-dacp | 0.17 ± 0.04 | |
| Cisplatin | — | — | 0.43 ± 0.06 | — | | | | | |

[a] Taken from ref. 10 and those within. [b] Tested as a perchlorate, rather than a chloride salt.

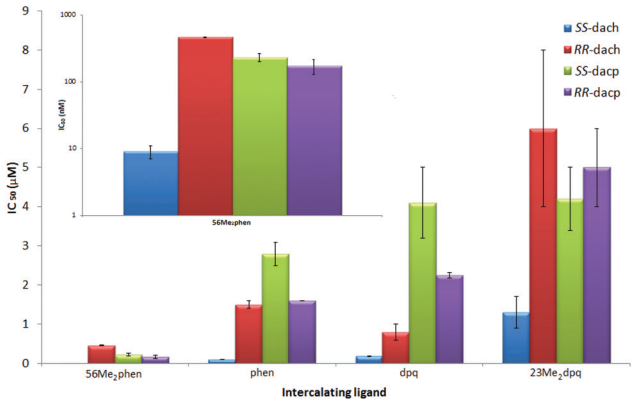


Fig. 8 Comparison of the *in vitro* cytotoxicity of complexes **1–16**, expressed as μM $IC_{50}$ values. Inset: the cytotoxicity of the $56Me_2$phen-incorporating complexes, expressed in nM using a logarithmic scale.

viously reported trends,[10] the complexes incorporating dach produced lower $IC_{50}$ values than those incorporating dacp.

Complexes **1–6** followed the same trend as the previously-reported complexes **11–18**; the *S*,*S* isomers of the dach-incorporating complexes were more active than the *R*,*R*, while the opposite was true for the complexes incorporating dacp. This confirms that the $A_L$ had more of an influence on the activity of these complexes than the $I_L$. The exceptions to these trends were complexes **7** and **8**, as they were approximately equal in cytotoxicity.

In general, each dpq derivative-incorporating complex was less cytotoxic than the phen derivate counterpart. Interestingly, the complexes incorporating dpq were much less active than those containing phen, despite the higher DNA binding affinity determined using FIDs. These results suggest that the DNA binding of these complexes is not the only intracellular interaction that contributes to their cytotoxicity, and supports the notion that the activity of these complexes arises from contributions of both the $I_L$ and $A_L$. An unexpected trend amongst the complexes tested was that the use of methylated $I_L$s resulted in much higher cytotoxicity for **9–16**, whereas the opposite effect was observed for **1–8**. It is clear that the presence of methyl substituents on the $I_L$ of PCs will not always result in higher levels of biological activity.

## Conclusion

Eight platinum complexes of the type $[Pt(I_L)(A_L)]Cl_2$, six of which are novel, were synthesised using an adaptation of published methods. The purity of each complex was determined *via* a variety of spectroscopic techniques. The CT-DNA binding affinities of these complexes were compared to those of the published complexes **9–16** through the use of fluorescent intercalator displacement assays. The order of binding affinity in relation to the $I_L$ used was $56Me_2$phen > $23Me_2$dpq = dpq > phen. These results indicate that an increased aromatic surface area and methylation of the $I_L$ may independently result in a higher DNA binding affinity; however a combination of these two characteristics is not guaranteed to produce higher efficacy. Due to different trends observed between this study and another,[11] further investigation is required in order to elucidate the true nature of PC-DNA binding in relation to the choice of $I_L$. Finally, each of complexes **1–8** were found to be cytotoxic to the L1210 cell line, with complex **1** being more active than cisplatin. Overall, the dpq-containing complexes were not as active as complexes **9–16**, although further testing in other cell lines may reveal different trends.

## Acknowledgements

The authors thank the University of Western Sydney for its financial support through internal research grants. B.J.P. was supported by an Australian Postgraduate Award and a UWS Top-Up Award. D.L.A. was supported by a UWS Honours Scholarship. We also thank Allan Torres for his helpful NMR discussions, and Jeffrey Reimers for access to his CNDO/S program. J.K.C. thanks the Australian Research Council for support.

## Notes and references

1 A. Jemal, F. Bray, M. M. Center, J. Ferlay, E. Ward and D. Forman, *CA-Cancer J. Clin.*, 2011, **61**, 69–90.
2 M. P. M. Marques, *ISRN Spectrosc.*, 2013, **2013**, 29–29.
3 B. H. Harper, F. Li, R. Beard, K. B. Garbutcheon-Singh, N. S. Ng and J. R. Aldrich-Wright, in *Supramolecular Systems in Biomedical Fields*, ed. H. J. Schneider, Royal Society of Chemistry, Cambridge, UK, 1st edn, 2013, ch. 9.
4 M. Kartalou and J. M. Essigmann, *Mutat. Res., Fundam. Mol. Mech. Mutagen.*, 2001, **478**, 23–43.
5 N. J. Wheate, S. Walker, G. E. Craig and R. Oun, *Dalton Trans.*, 2010, **39**, 8113–8127.
6 G. Momekov, A. Bakalova and M. Karaivanova, *Curr. Med. Chem.*, 2005, **12**, 2177–2191.
7 Z. Ma, J. R. Choudhury, M. W. Wright, C. S. Day, G. Saluta, G. L. Kucera and U. Bierbach, *J. Med. Chem.*, 2008, **51**, 7574–7580.
8 S. Komeda, *Metallomics*, 2011, **3**, 650–655.
9 K. Benjamin Garbutcheon-Singh, S. Myers, B. W. J. Harper, N. S. Ng, Q. Dong, C. Xie and J. R. Aldrich-Wright, *Metallomics*, 2013, **5**, 1061–1067.
10 K. B. Garbutcheon-Singh, P. Leverett, S. Myers and J. R. Aldrich-Wright, *Dalton Trans.*, 2013, **42**, 918–926.
11 S. Kemp, N. J. Wheate, D. P. Buck, M. Nikac, J. G. Collins and J. R. Aldrich-Wright, *J. Inorg. Biochem.*, 2007, **101**, 1049–1058.
12 D. Wilmanska, M. Czyz, K. Studzian, M. K. Piestrzeniewicz and M. Gniazdowski, *Z. Naturforsch., C: J. Biosci.*, 2001, **56**, 886–891.
13 A. M. Krause-Heuer, R. Grünert, S. Kühne, M. Buczkowska, N. J. Wheate, D. D. Le Pevelen, L. R. Boag, D. M. Fisher, J. Kasparkova, J. Malina, P. J. Bednarski, V. Brabec and J. R. Aldrich-Wright, *J. Med. Chem.*, 2009, **52**, 5474–5484.

 

14 C. R. Brodie, J. G. Collins and J. R. Aldrich-Wright, *Dalton Trans.*, 2004, 1145–1152.
15 D. Jaramillo, D. P. Buck, J. G. Collins, R. R. Fenton, F. H. Stootman, N. J. Wheate and J. R. Aldrich-Wright, *Eur. J. Inorg. Chem.*, 2006, **2006**, 839–849.
16 G. Arena, L. M. Scolaro, R. F. Pasternack and R. Romeo, *Inorg. Chem.*, 1995, **34**, 2994–3002.
17 F. H. Dickey, W. Fickett and H. J. Lucas, *J. Am. Chem. Soc.*, 1952, **74**, 944–951.
18 J. G. Collins, A. D. Sleeman, J. R. Aldrich-Wright, I. Greguric and T. W. Hambley, *Inorg. Chem.*, 1998, **37**, 3133–3141.
19 Agilent Technologies, Oxford Diffraction Ltd., 2009–2011.
20 A. Altomare, M. C. Burla, M. Camalli, G. L. Cascarano, C. Giacovazzo, A. Guagliardi, A. G. G. Moliterni, G. Polidori and R. Spagna, *J. Appl. Crystallogr.*, 1999, **32**, 115–119.
21 G. M. Sheldrick, *SHELXL-2013: Programs for Crystal Structure Analysis*, University of Göttingen, Germany, 2013.
22 L. J. Farrugia, *J. Appl. Crystallogr.*, 1999, **32**, 837–838.
23 T. Maniatis, E. F. Fritsch and J. Sambrook, *Molecular Cloning: A Laboratory Manual*, Cold Spring Harbor Laboratory, NY, USA, 1982.
24 C. Y. Lee, H.-W. Ryu and T.-S. Ko, *Bull. Korean Chem. Soc.*, 2001, **22**, 87–89.
25 N. J. Wheate, R. I. Taleb, A. M. Krause-Heuer, R. L. Cook, S. Wang, V. J. Higgins and J. R. Aldrich-Wright, *Dalton Trans.*, 2007, 5055–5064.
26 R. M. Silverstein and F. X. Webster, *Spectrometric identification of organic compounds*, Wiley, New York, USA, 1998.
27 E. Bednarek, J. Sitkowski, R. Kawecki, L. Kozerski, W. Bocian, L. Pazderski and W. Priebe, *Dalton Trans.*, 2008, 4129–4137.
28 B. M. Still, P. G. A. Kumar, J. R. Aldrich-Wright and W. S. Price, *Chem. Soc. Rev.*, 2007, **36**, 665–686.
29 K. S. Pitzer and W. E. Donath, *J. Am. Chem. Soc.*, 1959, **81**, 3213–3218.
30 J. Del Bene, H. H. Jaffé, R. L. Ellis and G. Kuehnlenz, *QCPE program no. 174*, Department of Chemistry, Indiana University, Bloomington, IN 47405, U.S.A., 1970.
31 M. J. Frisch, G. W. Trucks, H. B. Schlegel, G. E. Scuseria, M. A. Robb, J. R. Cheeseman, J. A. Montgomery Jr., T. Vreven, K. N. Kudin, J. C. Burant, J. M. Millam, S. S. Iyengar, J. Tomasi, V. Barone, B. Mennucci, M. Cossi, G. Scalmani, N. Rega, G. A. Petersson, H. Nakatsuji, M. Hada, M. Ehara, K. Toyota, R. Fukuda, J. Hasegawa, M. Ishida, T. Nakajima, Y. Honda, O. Kitao, H. Nakai, M. Klene, X. Li, J. E. Knox, H. P. Hratchian, J. B. Cross, V. Bakken, C. Adamo, J. Jaramillo, R. Gomperts, R. E. Stratmann, O. Yazyev, A. J. Austin, R. Cammi, C. Pomelli, J. W. Ochterski, P. Y. Ayala, K. Morokuma, G. A. Voth, P. Salvador, J. J. Dannenberg, V. G. Zakrzewski, S. Dapprich, A. D. Daniels, M. C. Strain, O. Farkas, D. K. Malick, A. D. Rabuck, K. Raghavachari, J. B. Foresman, J. V. Ortiz, Q. Cui, A. G. Baboul, S. Clifford, J. Cioslowski, B. B. Stefanov, G. Liu, A. Liashenko, P. Piskorz, I. Komaromi, R. L. Martin, D. J. Fox, T. Keith, M. A. Al-Laham, C. Y. Peng, A. Nanayakkara, M. Challacombe, P. M. W. Gill, B. Johnson, W. Chen, M. W. Wong, C. Gonzalez and J. A. Pople, Gaussian, Inc., Wallingford CT, 2004.
32 L. Ancarani-Rossiello, *Gazz. Chim. Ital.*, 1967, **97**, 1177–1183.
33 F. E. Lytle and D. M. Hercules, *J. Am. Chem. Soc.*, 1969, **91**, 253–257.
34 N. Armaroli, L. De Cola, V. Balzani, J.-P. Sauvage, C. O. Dietrich-Buchecker and J.-M. Kern, *J. Chem. Soc., Faraday Trans.*, 1992, **88**, 553–556.
35 T. Koshiyama and M. Kato, *Acta Crystallogr., Sect. C: Cryst. Struct. Commun.*, 2003, **59**, m446–m449.
36 C. R. Brodie, P. Turner, N. J. Wheate and J. R. Aldrich-Wright, *Acta Crystallogr., Sect. E: Struct. Rep. Online*, 2006, **62**, m3137–m3139.
37 D. M. Fisher, P. J. Bednarski, R. Grünert, P. Turner, R. R. Fenton and J. R. Aldrich-Wright, *ChemMedChem*, 2007, **2**, 488–495.
38 H. D. Flack, *Helv. Chim. Acta*, 2003, **86**, 905–921.
39 L. M. Salonen, M. Ellermann and F. Diederich, *Angew. Chem., Int. Ed.*, 2011, **50**, 4808–4842.
40 J. Nygren, N. Svanvik and M. Kubista, *Biopolymers*, 1998, **46**, 39–51.
41 E. Grueso, G. López-Pérez, M. Castellano and R. Prado-Gotor, *J. Inorg. Biochem.*, 2012, **106**, 1–9.
42 S. Shi, H.-L. Huang, X. Gao, J.-L. Yao, C.-Y. Lv, J. Zhao, W.-L. Sun, T.-M. Yao and L.-N. Ji, *J. Inorg. Biochem.*, 2013, **121**, 19–27.
43 R. W. Sabnis, *Handbook of Biological Dyes and Stains: Synthesis and Industrial Applications*, John Wiley & Sons, New Jersey, 2010.
44 J. B. Lepecq and C. Paoletti, *J. Mol. Biol.*, 1967, **27**, 87–106.
45 R. R. Monaco, *J. Biomol. Struct. Dyn.*, 2007, **25**, 119–125.
46 H. Zhao, M. Ge, Z. Zhang, W. Wang and G. Wu, *Spectrochim. Acta, Part A*, 2006, **65**, 811–817.
47 O. Stern and M. Volmer, *Phys. Z.*, 1919, **20**, 183–188.
48 D. P. Heller and C. L. Greenstock, *Biophys. Chem.*, 1994, **50**, 305–312.
49 W. R. Ware, *J. Phys. Chem.*, 1962, **66**, 455–458.
50 W. C. Tse and D. L. Boger, *Acc. Chem. Res.*, 2003, **37**, 61–69.
51 B. K. S. Yeung, W. C. Tse and D. L. Boger, *Bioorg. Med. Chem. Lett.*, 2003, **13**, 3801–3804.
52 S. P. Sau, P. Kumar, P. K. Sharma and P. J. Hrdlicka, *Nucleic Acids Res.*, 2012, **40**, e162.
53 S. M. Kelly, T. J. Jess and N. C. Price, *Biochim. Biophys. Acta, Proteins Proteomics*, 2005, **1751**, 119–139.
54 N. J. Wheate, C. R. Brodie, J. G. Collins, S. Kemp and J. R. Aldrich-Wright, *Mini-Rev. Med. Chem.*, 2007, **7**, 627–648.
55 N. Shahabadi and L. Heidari, *Spectrochim. Acta, Part A*, 2014, **128**, 377–385.